Advances in Science and Technology Research Journal

Advances in Science and Technology Research Journal, 2025, 19(10), 444–460
https://doi.org/10.12913/22998624/208946
ISSN 2299-8624, License CC-BY 4.0

Received: 2025.05.30
Accepted: 2025.08.15
Published: 2025.09.01

Adaptive robust iterative backstepping control for pump-driven electro-hydraulic rotary actuator

Dao Thanh Liem[1], Nguyen Minh Tri[2*]

[1] Faculty of Mechanical Technology, Ho Chi Minh City University of Industry and Trade, 140 Le Trong Tan, Ho Chi Minh City, Vietnam
[2] Faculty of Engineering and Technology, Nguyen Tat Thanh University, Ho Chi Minh, Vietnam
* Corresponding author's e-mail: nmtri@ntt.edu.vn

ABSTRACT

Electro-hydraulic actuators (EHAs) are increasingly used in modern industrial systems due to their compact design, energy efficiency, and high precision, offering a sustainable alternative to traditional valve-controlled hydraulic systems (VHS). However, conventional control methods such as PID and sliding mode control often fall short in ensuring robust performance in pump-driven EHA systems with rotary actuators, due to strong nonlinearities, parameter uncertainties, and unmeasurable internal states. This study introduces a novel position control method for electro-hydraulic rotary actuator systems (EHRAs) by integrating a modified backstepping algorithm, an iterative learning control (ILC) scheme, and a nonlinear state observer. The control strategy is developed based on Lyapunov stability theory to ensure robustness and convergence under varying operating conditions. A co-simulation using MATLAB/Simulink and AMESim was carried out to validate the control strategy. Quantitative results show that the proposed method achieves superior tracking accuracy with a position error below 0.5% and state estimation errors within 1% after 0.2 seconds. Simulation results indicate that the proposed control strategy maintains accurate tracking and remains stable under external disturbances. This study is the first to combine modified backstepping, ILC, and nonlinear observation for rotary EHAs. The stability of the proposed solution highlights its potential for use in high-precision motion control applications in robotics, aerospace systems, and heavy industry.

Keywords: electro–hydraulic rotary actuator, hydraulic system, backstepping control, iterative learning, tracking control.

INTRODUCTION

Hydraulic systems remain essential in modern industry due to their reliability and ability to generate substantial force. Many different fields use these systems, like manufacturing, aerospace, robotics, heavy equipment, and automotive engineering [1–3]. Most hydraulic systems, especially valve-controlled hydraulic systems (VHSs), direct fluid through valves to control actuator motion and provide force. However, VHSs have some problems, like polluting the environment when they leak, needing a lot of maintenance, being heavy, and having a lot of space to install [4]. To overcome the limitations associated with valve-based systems, pump-controlled EHAs have emerged as a popular alternative, particularly in applications where accuracy and efficiency are crucial. EHAs are like power converters that use a bidirectional pump to change the high speed of an electric motor into hydraulic power for a hydraulic actuator. EHAs provide a more compact, cleaner, and energy-efficient solution for generating high force by directly controlling the actuator via the supply pump [5, 6].

Rotary actuators (RAs) play a critical role in industrial applications where high torque output is required within constrained spatial environments. Among these, vane-type actuators are particularly favored due to their ability to deliver substantial torque in compact configurations, making them ideal for integration in robotics,

automated systems, and precision machinery [7–8]. Despite their advantages, achieving precise position tracking with RAs remains a complex task. This difficulty stems from nonlinear fluid dynamics and system uncertainties, including fluid compressibility, pressure fluctuations, flow turbulence, and mechanical imperfections such as backlash, variable friction, and seal degradation. In addition, temperature and pressure variations can lead to changes in the effective bulk modulus of the hydraulic fluid, further complicating dynamic system behavior. These factors collectively hinder system stability and control accuracy, especially when the actuator is subjected to fluctuating loads. Consequently, the design of control strategies that are both robust to nonlinearity and adaptive to uncertainty continues to be a major focus in the control of rotary actuators [9–11].

Controlling pump-driven EHAs presents challenges due to the tightly coupled dynamics of multiple system components. In contrast to valve-based systems, where control efforts primarily target fluid flow modulation via a servo valve, pump-controlled configurations must simultaneously account for the interaction between the bidirectional pump, the associated control valve, and the hydraulic actuator itself [12]. The nonlinear pressure–flow characteristics of the pump, along with variable motor speed and fluid compressibility, contribute to transient pressure fluctuations. These effects become especially prominent under varying load conditions. The performance of the system behavior becomes even more unpredictable due to internal leakage, friction, and sensitivity to thermal and pressure variations, all of which affect the bulk modulus of the hydraulic fluid. These time-varying and nonlinear effects make precise position control a challenging task, demanding more advanced and adaptive control strategies [13–15].

To address these complexities, several control approaches have been proposed. PID controllers remain popular due to their simplicity, but their fixed gains limit performance under variable operating conditions. Fuzzy-PID controllers offer greater adaptability but rely heavily on expert-defined rule sets, which may lack robustness outside expected conditions [16–21]. Sliding Mode Control (SMC) is known for its robustness to uncertainties; however, its inherent high-frequency switching behavior can degrade actuator performance, particularly in precision-critical applications such as robotics and aerospace systems [22–24]. Adaptive backstepping, though effective in structured nonlinear systems, may lose performance if the system includes unmodeled dynamics or varying parameters [25–26]. More recently, model predictive control (MPC) has shown potential, but its high computational load and strong dependence on accurate models can limit real-time embedded systems [27–28]. These limitations indicate the need for a more resilient and flexible control framework tailored to the complex behavior of pump-driven EHAs in practical applications.

To overcome the above drawbacks, this paper proposes a position control strategy for pump-driven EHRAs, aiming to improve tracking accuracy and robustness under practical industrial conditions. The system is composed of a pump-controlled unit and a vane-type rotary actuator, providing compact, high-torque rotational motion suitable for robotic and heavy-duty automation applications. To develop the control framework, a nonlinear dynamic model is established that captures the coupled behavior of the bidirectional pump, rotary actuator, and internal fluid dynamics, while also accounting for disturbances such as friction, load variation, and temperature-induced changes in fluid properties. A hybrid controller is introduced, integrating a modified backstepping algorithm, iterative learning control (ILC), and a nonlinear state observer. The backstepping component provides a stabilizing control law through recursive virtual inputs, supported by Lyapunov-based analysis to ensure system stability. ILC enhances tracking performance by updating the control input across repetitive trajectories, improving accuracy under cyclic motion conditions [29]. Since direct measurement of some internal states – such as chamber pressures – is impractical, a Luenberger-like observer is employed to estimate these variables using available position and velocity data [30]. While ILC has been applied in other domains, its combined use with backstepping and observation in EHA control remains limited. This study addresses that gap, validating the proposed approach through simulations under various conditions, including load variations (up to 50%), external disturbances, and trajectory frequencies from 0.1 to 1 Hz.

SYSTEM MODELING AND PROBLEM STATEMENT

The EHRA system investigated in this study is a pump-driven system designed for precise

position control in industrial applications. The EHRA system consists of a gear pump, an additional valve system, and a bidirectional symmetrical hydraulic rotary cylinder. The gear pump, driven by an electric motor, delivers hydraulic power by controlling fluid flow to the actuator. To regulate pressure levels and maintain safe operation across a range of load conditions, a valve system is integrated into the circuit. The rotary actuator then transforms the supplied hydraulic pressure into rotational motion, generating the torque required for the intended application. Figure 1 illustrates the system architecture, including the functional connections between the pump, valves, and actuator.

The dynamics of the EHRA system are modeled in state-space form to facilitate the design of the proposed control strategy. The state variables are defined as follows:

$$\begin{aligned} \alpha_1 &= y \\ \alpha_2 &= \dot{y} \\ \alpha_{34} &= \frac{A}{m}(\alpha_3 - \alpha_4) \end{aligned} \tag{1}$$

where: α_1 represents the angular position of the rotary cylinder in radians (rad), α_2 denotes the angular velocity in radians per second (rad/s) and α_{34} captures the scaled pressure difference in meters per second squared (m/s²), $\alpha_3 = P_1$, $\alpha_4 = P_2$ are the pressures in chambers 1 and 2, respectively. The state-space representation of the EHRA system dynamics, as derived from first principles and simplified for control design, is given by the following equations:

$$\begin{aligned} \dot{\alpha}_1 &= \alpha_2 \\ \dot{\alpha}_2 &= \alpha_{34} + d \\ \dot{\alpha}_{34} &= \frac{m\beta(V_{01} + V_{02})}{A(V_{01} + A\alpha_1)(V_{02} - A\alpha_1)} \\ & (D\omega - k_l\alpha_{34} - A\alpha_2) + Q_v \end{aligned} \tag{2}$$

where: J – moment of inertia of the rotary system (kg·m²), A – effective area parameter (related to D_R / r, assumed consistent with units), m – equivalent mass parameter adjusted for rotary motion (kg), $d = -\frac{F_r}{m}$ – external disturbance term (m/s²), F_r – external force, β – effective bulk modulus (adjusted as $\frac{A\beta_e}{m}$), $k_l = \frac{m}{A}k_{\text{leakage}}$ – scaled leakage coefficient, representing internal leakage between the cylinder chambers, D – pump displacement (m³/rad), defining the volume of fluid displaced per radian of pump rotation, ω – pump speed (rad/s, control input), which serves as the control input to the system, V_{01}, V_{02}–initial chamber volumes (m³), $Q_v = \frac{m}{A}\left(\frac{\beta Q_{v1}}{V_{01} + A\alpha_1} - \frac{\beta Q_{v2}}{V_{02} - A\alpha_1}\right)$ – valve flow term (assumed negligible or zero for simplicity in this design), Q_{v1}, and Q_{v2} are flow rates through valves v_1, and v_2 respectively. The function encapsulates the nonlinear pressure dynamics of the system and is defined as:

$$f(\alpha_1) = \frac{m\beta(V_{01}+V_{02})}{A(V_{01}+A\alpha_1)(V_{02}-A\alpha_1)} \tag{3}$$

$$g = f(\alpha_1)D \tag{4}$$

To prevent numerical issues during simulation, such as division by zero, the denominators are bounded by a small positive constant. Substituting $f(\alpha_1)$ into the pressure dynamics equation, the evolution of the pressure dynamics α_{34} becomes:

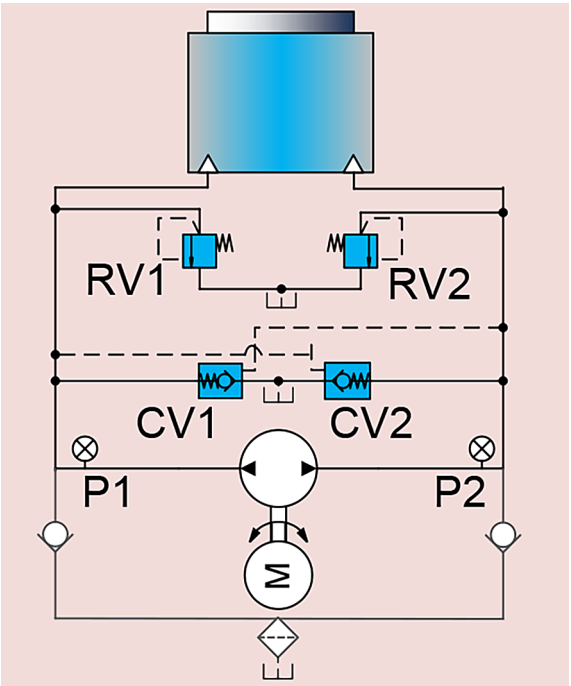

Figure 1. Structure of the EHRA system, source: https://www.boschrexroth.com

$$\dot{\alpha}_{34} = f(\alpha_1)$$
$$= \frac{(-k_l\alpha_{34} - A\alpha_2) + g\omega}{\frac{m\beta(V_{01}+V_{02})}{A(V_{01}+A\alpha_1)(V_{02}-A\alpha_1)}(-k_l\alpha_{34} - A\alpha_2) + \frac{m\beta(V_{01}+V_{02})D\omega}{A(V_{01}+A\alpha_1)(V_{02}-A\alpha_1)}} \quad (5)$$

This formulation highlights the nonlinear dependency of the pressure dynamics on the angular position α_1, as well as the direct influence of the control input ω on the performance of the system behavior. The presence of the uncertain parameter k_1, which varies with operating conditions such as temperature and wear, and the external disturbance d, which may include unmodeled friction or load variations, further complicates the control design. The primary control objective is to design the pump speed ω such that the angular position α_1 tracks a bounded desired trajectory α_{1d} (t), which is assumed to be at least twice differentiable with bounded derivatives. This ensures that the reference trajectory and its derivatives and acceleration are physically realizable for the EHRA system. In addition, the control strategy must adaptively estimate the uncertain parameter to account for leakage variations and robustly compensate for external disturbances d to maintain tracking performance under various operating conditions. Integrating a state observer, as part of the proposed hybrid control framework, further ensures that the unmeasured states are accurately estimated, enabling effective feedback control despite the nonlinearities and uncertainties of the system.

CONTROL DESIGN

The design of the adaptive robust iterative backstepping controller utilizes the backstepping method, a recursive control technique that is particularly well suited to nonlinear systems in a strict feedback form, such as the EHRA system described by state-space equations [31-33]. This approach systematically constructs the control law by breaking down the system dynamics into a series of subsystems, identifying virtual control inputs and error variables at each level, and ensuring global stability through the use of Lyapunov functions. Specifically, the backstepping design addresses the nonlinear dynamics of the EHRA by treating the states as a sequence, where each state is recursively stabilized relative to the previous state. To address the challenges posed by parameter uncertainty and external disturbances, the controller integrates an adaptive mechanism for online parameter estimation and a disturbance observer for robust compensation. The adaptive mechanism employs a projection-based update law to estimate k_1, ensuring that the estimated parameter remains within physically meaningful bounds, while the disturbance observer, designed using a nonlinear observer framework, provides an estimate of d to mitigate its impact on tracking performance. Furthermore, to enhance the functionality of the controller ability to track periodic trajectories, an iterative learning scheme is incorporated, which adjusts the control input over successive iterations based on the tracking error, complementing the backstepping and adaptive components.

The primary control objective is to regulate the angular position α_1 of the EHRA system to accurately track a predefined, bounded reference trajectory α_{1d}, thereby ensuring high-precision motion control suitable for industrial environments. The reference trajectory α_{1d} is assumed to be sufficiently smooth, specifically at least twice differentiable with bounded derivatives, to facilitate the derivation of the control law and ensure physical realizability of the desired motion. The EHRA system, as described by the state-space equations in previous section, is a third-order nonlinear system characterized by the state variables α_1, α_2, α_{34}, which collectively capture the position, velocity, and pressure dynamics of the hydraulic rotary actuator. The backstepping design process, tailored for systems in strict feedback form, begins by stabilizing the outermost state α_1, treating the subsequent state α_2 as a virtual control input to regulate the position error dynamics. This recursive approach ensures that the tracking error is systematically minimized while maintaining system stability through Lyapunov-based techniques. To quantify the tracking performance, the position error is defined as the deviation of the actual angular position from the desired trajectory:

$$z_1 = \alpha_1 - \alpha_{1d} \quad (6)$$

To design the control law, compute the time derivative of z_1 to understand how the error evolves:

$$\dot{z}_1 = \frac{d}{dt}(\alpha_1 - \alpha_{1d}) = \\ = \dot{\alpha}_1 - \dot{\alpha}_{1d} = \alpha_2 - \dot{\alpha}_{1d} \quad (7)$$

Here, $\dot{\alpha}_{1d}$ is the desired angular velocity, assumed to be known and computable from the reference trajectory α_{1d}. The equation reveals that the evolution of the position error z_1 depends directly on the actual velocity α_2, which is the next state in the system hierarchy. In the backstepping framework, α_2 is treated as a virtual control input to stabilize z_1. The objective is to define a desired value for α_2, denoted α_{2d}, such that if $\alpha_2 = \alpha_{2d}$, the error z_1 converges to zero. To achieve this, propose a virtual control law inspired by feedback stabilization:

$$\alpha_{2d} = \dot{\alpha}_{1d} - k_1 z_1 \tag{8}$$

where: k_1 – positive control gain ($k_1 > 0$), to be selected later for tuning the convergence rate. Since α_2 is a system state and not directly manipulable, define the velocity error as the difference between the actual velocity and the desired virtual control:

$$z_2 = \alpha_2 - \alpha_{2d} \tag{9}$$

$$\begin{gathered} \dot{z}_1 = \alpha_2 - \dot{\alpha}_{1d} = \\ = (z_2 + \alpha_{2d}) - \dot{\alpha}_{1d} = \\ = z_2 + (\dot{\alpha}_{1d} - k_1 z_1) - \\ - \dot{\alpha}_{1d} = z_2 - k_1 z_1 \end{gathered} \tag{10}$$

This resulting differential equation governs the dynamics of the position error z_1, now expressed as a function of the velocity error z_2 and a stabilizing term proportional to z_1. To ensure that the virtual control α_{2d} stabilizes z_1 when $\alpha_2 = \alpha_{2d}$ (i.e., $z_2 = 0$), construct a Lyapunov function candidate, which is a standard tool for assessing stability in control systems:

$$V_1 = \frac{1}{2} z_1^2 \tag{11}$$

Compute its time derivative to evaluate the performance of the system behavior:

$$\begin{gathered} \dot{V}_1 = \frac{d}{dt}\left(\frac{1}{2} z_1^2\right) = \frac{\partial V_1}{\partial z_1} \dot{z}_1 = \\ = z_1 \dot{z}_1 = z_1 (z_2 - k_1 z_1) \end{gathered} \tag{12}$$

$$\dot{V}_1 = -k_1 z_1^2 \tag{13}$$

This is negative definite, implying that $z_1 \to 0$ exponentially with a rate determined by k_1. Specifically, the dynamics become:

$$\dot{z}_1 = -k_1 z_1 \tag{14}$$

The solution is:

$$z_1(t) = z_1(0) e^{-k_1 t} \tag{15}$$

Since $k_1 > 0$, $z_1 \to 0$, confirming the effectiveness of α_{2d} as a stabilizing virtual control. Define the velocity error as the deviation of the actual angular velocity from the desired virtual control:

$$z_2 = \alpha_2 - \alpha_{2d} = \alpha_2 - (\dot{\alpha}_{1d} - k_1 z_1) \tag{16}$$

To design a control law for z_2, compute its time derivative:

$$\begin{gathered} \dot{z}_2 = \frac{d}{dt}(\alpha_2 - \alpha_{2d}) = \dot{\alpha}_2 - \dot{\alpha}_{2d} \\ = \alpha_{34} + d - \ddot{\alpha}_{1d} + k_1 z_2 - k_1^2 z_1 \end{gathered} \tag{17}$$

This equation shows that $\dot{z}_2$ depends on the pressure state α_{34}, the disturbance d, and terms involving z_1 and z_2, reflecting the performance of the system hierarchical structure. Treat α_{34} as a virtual control input to stabilize z_2. The goal is to define a desired pressure difference α_{34d} such that if $\alpha_{34} = \alpha_{34d}$ z_2 converges to zero, neutralizing the $z_1 z_2$ term in $\dot{V}_1$. Propose:

$$\begin{gathered} \alpha_{34d} = -z_1 - k_2 z_2 - \\ - d + \ddot{\alpha}_{1d} - k_1 z_2 + k_1^2 z_1 \end{gathered} \tag{18}$$

where: $k_2 > 0$ is a positive control gain. However, since the disturbance d is unknown in practice, a nonlinear observer is introduced to estimate it. Let $\hat{d}$ denote the estimated disturbance. The virtual control law is then modified by substituting $\hat{d}$ in place of the unknown d to ensure implementability:

$$\begin{gathered} \alpha_{34d} = -z_1 - k_2 z_2 - \hat{d} + \ddot{\alpha}_{1d} - \\ - k_1 z_2 + k_1^2 z_1 \end{gathered} \tag{19}$$

Define the pressure error:

$$z_3 = \alpha_{34} - \alpha_{34d} \tag{20}$$

Substitute into the velocity error dynamics:

$$\begin{gathered} \dot{z}_2 = (z_3 + \alpha_{34d}) + d - \\ - \ddot{\alpha}_{1d} + k_1 z_2 - k_1^2 z_1 = z_3 + \\ + \left(-z_1 - k_2 z_2 - \hat{d} + \ddot{\alpha}_{1d} - k_1 z_2 + k_1^2 z_1\right) + \\ + d - \ddot{\alpha}_{1d} + k_1 z_2 - k_1^2 z_1 = \\ = z_3 - z_1 - k_2 z_2 - \hat{d} + d = \\ = z_3 - z_1 - k_2 z_2 + \tilde{d} \end{gathered} \tag{21}$$

where: $\tilde{d} = d - \hat{d}$ is disturbance estimation error. To estimate d, design a disturbance observer assuming d is slowly varying $(\dot{d} \approx 0)$. Propose an observer dynamics:

$$\dot{\hat{d}} = -l(\hat{d} + \alpha_{34} - \dot{\alpha}_2) \tag{22}$$

where: $l > 0$ is the observer gain. Compute the error dynamics:

$$\dot{\tilde{d}} = -l(d - \hat{d}) = -l\tilde{d} \tag{23}$$

This is a first-order system with solution $\tilde{d}(t) = \tilde{d}(0)e^{-lt}$. Since $l > 0$, $\tilde{d} \to 0$ exponentially, ensuring $\hat{d} \to d$ over time. In practice, $\dot{\alpha}_2$ is approximated numerically (e.g., $\dot{\alpha}_2 \approx \frac{\alpha_2(t) - \alpha_2(t - \Delta t)}{\Delta t}$), which introduces minor estimation errors but is manageable with a small time step. Augment the Lyapunov function from Step 1 to include the velocity error and disturbance estimation error:

$$V_2 = V_1 + \frac{1}{2}z_2^2 + \frac{1}{2l}\tilde{d}^2 = \frac{1}{2}z_1^2 + \frac{1}{2}z_2^2 + \frac{1}{2l}\tilde{d}^2 \tag{24}$$

Compute its derivative:

$$\dot{V}_2 = -k_1 z_1^2 - k_2 z_2^2 + z_2 z_3 + z_2\tilde{d} - \tilde{d}^2 \tag{25}$$

Bound the cross-term using Young's inequality

$$(ab \le \frac{a^2}{2} + \frac{b^2}{2}):\ z_2\tilde{d} \le \frac{1}{2}z_2^2 + \frac{1}{2}\tilde{d}^2$$

$$\dot{V}_2 \le -k_1 z_1^2 - (k_2 - \frac{1}{2})z_2^2 + z_2 z_3 - \frac{1}{2}\tilde{d}^2 \tag{26}$$

If $z_3 = 0$ and $k_2 > \frac{1}{2}$:

$$\dot{V}_2 \le -k_1 z_1^2 - (k_2 - \frac{1}{2})z_2^2 - \frac{1}{2}\tilde{d}^2 \tag{27}$$

The Lyapunov derivative shows that stability depends on controlling z_3 and the estimation of the observer performance. The disturbance observer ensures $\tilde{d} \to 0$, mitigating the $z_2\tilde{d}$ term over time. The $z_2 z_3$ term requires the next step, where α_{34} is regulated via the pump speed ω, incorporating adaptive estimation of k_l. The gains k_2 and l are chosen to ensure $k_2 > \frac{1}{2}$ and fast disturbance rejection, balanced against noise sensitivity in practical implementation. This step advances the design by stabilizing the velocity subsystem, paving the way for the final pressure dynamics. Define the observer dynamics:

$$\dot{\hat{d}} = -l(\hat{d} + \alpha_{34} - \dot{\alpha}_2) \tag{28}$$

Since $\dot{\alpha}_2$ is not directly measured, use the system equation:

$$\dot{\hat{d}} = -l(\hat{d} + \alpha_{34} - (\alpha_{34} + d)) \tag{29}$$

Substitute into $\dot{V}_2$:

$$\dot{V}_2 = -k_1 z_1^2 - k_2 z_2^2 + z_2 z_3 + z_2\tilde{d} - \tilde{d}^2 \tag{30}$$

Compute the time derivative of z_3:

$$\dot{z}_3 = \frac{d}{dt}(\alpha_{34} - \alpha_{34d}) \tag{31}$$

From the system model:

$$\dot{\alpha}_{34} = \frac{m\beta(V_{01} + V_{02})}{A(V_{01} + A\alpha_1)(V_{02} - A\alpha_1)} (D\omega - k_l\alpha_{34} - A\alpha_2) + Q_v \tag{32}$$

Differentiate:

$$\begin{aligned}\dot{\alpha}_{34d} &= -\dot{z}_1 - k_2\dot{z}_2 - \dot{\hat{d}} + \\ &+\ddot{\alpha}_{1d} - k_1\dot{z}_2 + k_1^2\dot{z}_1 \\ &= k_1(2 + k_2 - k_1^2)z_1 + \\ &+ (-1 + k_2^2 + k_1 k_2 + k_1^2)z_2 - \\ &-(k_1 + k_2)z_3 + \\ &+ (-k_1 - k_2 - l)\tilde{d} + \ddot{\alpha}_{1d}\end{aligned} \tag{33}$$

This exact form is complex for real-time computation, so in practice, $\dot{\alpha}_{34d}$ is approximated numerically (e.g., $\dot{\alpha}_{34d} \approx \frac{\alpha_{34d}(t) - \alpha_{34d}(t - \Delta t)}{\Delta t}$.

Substitute into $\dot{z}_3$:

$$\dot{z}_3 = f(\alpha_1)(-k_l\alpha_{34} - A\alpha_2) + g\omega - \dot{\alpha}_{34d} \tag{34}$$

Design ω to stabilize z_3

$$\omega = \frac{1}{g}\begin{bmatrix} -z_2 - k_3 z_3 - f(\alpha_1) \\ (-\hat{k}_l\alpha_{34} - A\alpha_2) + \dot{\alpha}_{34d} \end{bmatrix} \tag{35}$$

$$\dot{z}_3 = -z_2 - k_3 z_3 - f(\alpha_1)\tilde{k}_l\alpha_{34} \tag{36}$$

Augment the Lyapunov function:

$$V_3 = V_2 + \frac{1}{2}z_3^2 + \frac{1}{2\gamma}\tilde{k}_l^2 \tag{37}$$

$$\dot{V}_3 = -k_1 z_1^2 - k_2 z_2^2 - k_3 z_3^2 - \\ -z_3 f(\alpha_1)\tilde{k}_l \alpha_{34} + z_2\tilde{d} - \tilde{d}^2 + \frac{\tilde{k}_l \dot{\tilde{k}}_l}{\gamma} \tag{38}$$

Let's define:

$$\frac{\tilde{k}_l \dot{\tilde{k}}_l}{\gamma} = z_3 f(\alpha_1)\tilde{k}_l \alpha_{34} \tag{39}$$

$$\dot{V}_3 = -k_1 z_1^2 - k_2 z_2^2 - k_3 z_3^2 + z_2\tilde{d} - \tilde{d}^2 \tag{40}$$

Bound $\tilde{d}$ as:

$$z_2\tilde{d} \le \frac{1}{2}z_2^2 + \frac{1}{2}\tilde{d}^2 \tag{41}$$

$$\dot{V}_3 \le -k_1 z_1^2 - (k_2 - \frac{1}{2})z_2^2 - k_3 z_3^2 - \frac{1}{2}\tilde{d}^2 \tag{42}$$

If $k_2 > \frac{1}{2}$, $\dot{V}_3 \le 0$, ensuring all errors (z_1,z_2,z_3, $\tilde{d}$,$\tilde{k}_l$) are bounded and converge to zero asymptotically. Employing a modified ILC scheme, the control signal for the EHA system in the k^{th} iteration is defined as follows:

$$\omega_{(k)}(t) = \Gamma\,\omega_{(k-1)}(t) + \omega^*_{(k)}(t) \tag{43}$$

where: $\Gamma \in (0,1]$ is the adaptation gain, a scalar parameter that governs the influence of the previous iteration's control input on the current iteration; $\omega_{(k-1)}$ represents the control input (pump speed in rad/s) from the $(k-1)^{th}$.

SYSTEM EVALUATION SETUP

To implement and evaluate the performance of the proposed controller, a co-simulation platform integrating the EHRA system is established using AMESim and MATLAB/Simulink with an ODE solver. This co-simulation approach leverages the strengths of both tools: AMESim provides a high-fidelity physical model of the hydraulic components, while MATLAB/Simulink facilitates the implementation and tuning of the advanced control algorithms. Figures 2 and 3 illustrate the structure of the evaluation system, highlighting the interconnection between the physical model developed in AMESim and the control algorithm implemented in MATLAB/Simulink. In this study, the EHRA system is modeled in AMESim, comprising a gear pump, a bidirectional symmetrical hydraulic rotary actuator, and a supplementary valve assembly. The gear pump, driven by an electric motor, regulates the hydraulic fluid supplied to the rotary actuator, while the valve system maintains pressure stability and ensures safe operation under varying load conditions.

In addition to the system modeling, several evaluation assumptions and controller settings were adopted to ensure consistency and practical relevance. The reference trajectory was defined as continuous, bounded, and twice differentiable to support Lyapunov-based analysis and iterative learning. External disturbances were modeled as bounded and slowly varying, while key parameters such as the bulk modulus and internal leakage were assumed to be bounded and estimable.

Controller parameters were selected based on stability criteria and tuned through simulation. Feedback gains k_1, k_2, k_3 were chosen within 5–100 to ensure convergence without overshoot. The observer gain l ranged from 10 to 100, and the ILC learning rate Γ was set within (0, 1], typically between 0.3 and 0.8. These values were validated under varying trajectories and load conditions.

In the co-simulation setup, the pump speed ω, which serves as the control input, directly governs the rotational motion of the hydraulic rotary cylinder, as dictated by the dynamics in equation. To evaluate the robustness of the controller under realistic operating conditions, external disturbances are introduced to the system. A variable load was applied using a torque generator connected to the rotary cylinder, capable of adjusting the external force Fr, thereby influencing the disturbance term $d = -F_r/m$, simulating real-world scenarios such as load variations in industrial applications. Additionally, a friction model is incorporated into the AMESim simulation, with adjustable friction parameters to account for uncertainties in the contact. The motion of the rotary actuator is monitored using a high-precision angular encoder, which provides real-time measurements of the angular position α_1 and velocity α_2, while a pressure sensor measures the pressures P_1 and P_2

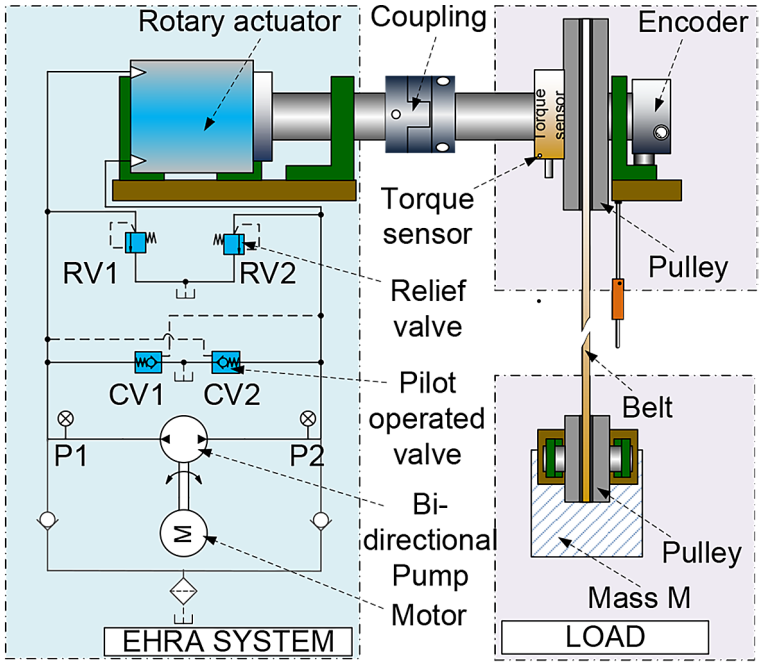

Figure 2. Structure of the evaluation system, designed using MS Visio

in the cylinder chambers to compute the scaled pressure difference α_{34}. These measurements are fed back to the MATLAB/Simulink environment for use in the state observer and control law computation. The designed control method, including the backstepping controller, the ILC scheme, and the state observer, is implemented in MATLAB/Simulink. The control law calculates the pump speed at each iteration and interfaces with the AMESim model through the co-simulation interface. An ODE solver is used to solve the system dynamics, ensuring numerical accuracy and stability during the simulation. The co-simulation runs for a total duration of 100 seconds, allowing a detailed evaluation of the controller performance in tracking the desired trajectory. Various operating conditions, including disturbances and parameter uncertainties, are included to evaluate the robustness and adaptability of the controller.

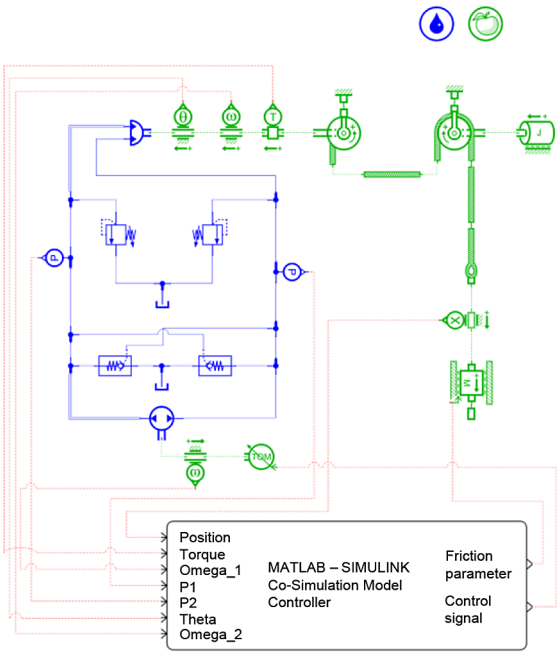

Figure 3. Schematic diagram of the EHRA system in the co-simulation platform, source: designed using MATLAB/Simulink and AMESim co-simulation

VALIDATION RESULTS

To evaluate the performance of the Iterative Backstepping Observer-based Controller (IBSOC), a sinusoidal reference trajectory was employed, and the results are presented in Figures 4 through 8. Additionally, external disturbances, including white noise and sinusoidal noise, were introduced to assess the robustness of the system. Initially, the traditional PID controller was simulated, and its performance is shown with double dot-dashed green lines. Due to fixed gains, it exhibited significant oscillations and errors, leading to a sluggish and unstable response during high activity. This is evident in the position responses shown in Figure 4 and the tracking errors displayed in Figure 5, both

using the same line style. The fixed-gain nature of the PID controller limited its adaptability under dynamic conditions.

Next, the FPID controller was tested under identical reference and noise conditions, with its performance indicated by short-dashed green lines. As shown in Figure 4, the FPID controller improved position tracking compared to the PID controller; however, the fuzzy inference mechanism of the FPID struggled to handle varying conditions, resulting in persistent tracking errors, as illustrated in Figure 5 using the same line style. The FSMC controller, represented by double dot-dashed purple lines, outperformed both PID and FPID controllers, yet it still produced oscillations and errors under substantial noise, as illustrated in Figure 5. Similarly, the IBSC controller, marked by dash-dotted blue lines, offered better steady-state error performance due to its iterative learning capabilities, which are visible in Figure 4. However, oscillations persisted, particularly in initial cycles, and errors remained large during reference signal direction changes, as shown in Figure 5 with the same line style.

To address these challenges, the IBSOC controller, described in Section 2, was implemented. Its trajectory tracking, marked by dashed red lines, is shown in Figure 4 and demonstrates superior speed, accuracy, and stability compared to other methods. The corresponding tracking errors, displayed in Figure 5 with the same line style, were minimal. Additionally, the control signal for the motor driving the hydraulic pump is presented in Figure 6, and the actuator chamber pressures are shown in Figure 7. By leveraging the IBSC framework and a self-tuning observer, the IBSOC effectively mitigated disturbances through compensatory actions, consistently outperforming the PID, FPID, FSMC, and IBSC controllers in speed, precision, and stability. This case clearly highlights the IBSOC's robustness for sinusoidal trajectories.

Next, a chirp reference trajectory (defined by a sinusoidal signal with varying frequency) was used to evaluate each controller's adaptability to dynamic changes. The corresponding results are presented in Figures 8 through 11. The PID controller, represented by double dot-dashed green

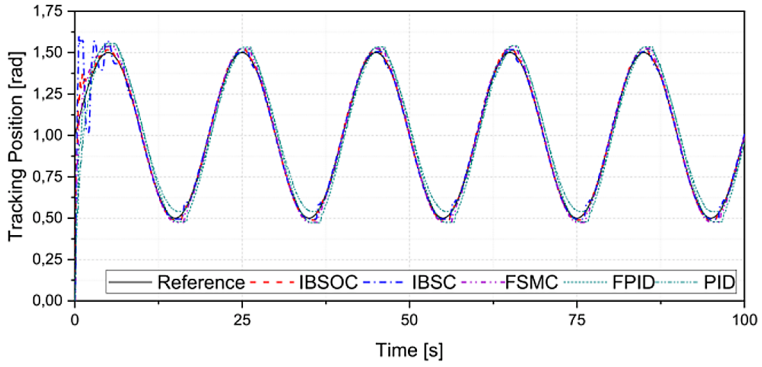

Figure 4. Comparison of tracking performance for a sinusoidal reference using different controllers, source: based on MATLAB/Simulink and AMESim co-simulation

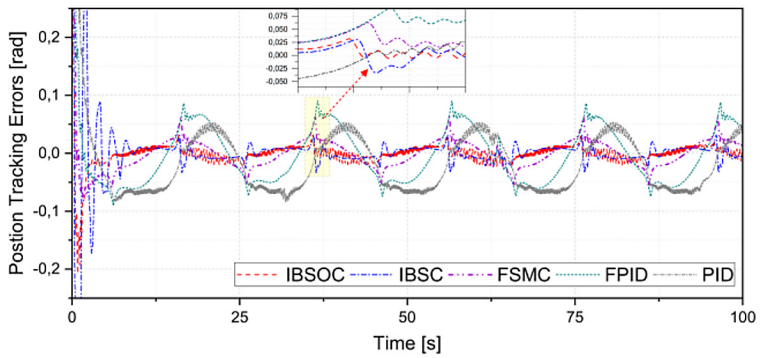

Figure 5. Comparison of tracking errors for a sinusoidal reference using different controllers, source: based on MATLAB/Simulink and AMESim co-simulation

lines, exhibited considerable instability during high-frequency phases, leading to large oscillations and tracking errors, as shown in Figure 8. Due to its fixed gains, the PID controller was unable to cope with the frequency variations of the input trajectory. The FPID controller, shown with short dashed green lines, demonstrated slight improvement in tracking performance; however, its limited adaptability resulted in unacceptable errors under varying conditions, as also seen in Figure 8. The FSMC controller, depicted by double dot-dashed purple lines, performed better than both PID and FPID controllers but still displayed noticeable oscillations and elevated errors under disturbance conditions. The IBSC controller, marked with dash-dotted blue lines, improved steady-state error and response due to its iterative learning mechanism, as illustrated in Figure 8. Nonetheless, residual oscillations were observed during the initial cycles and frequency transitions. In contrast, the IBSOC controller, identified by dashed red lines, delivered the most stable and precise response, as evidenced in Figure 8. The corresponding tracking errors in Figure 9 were the lowest among all evaluated controllers. Additionally, motor control signals and actuator chamber pressures are illustrated in Figures 10 and 11, respectively. These results underscore the superior adaptability and robustness of the IBSOC controller in handling frequency-varying trajectories within electro-hydraulic systems.

In addition, the multistep trajectory, widely used in industrial applications, was tested to evaluate the controllers' performance during abrupt position changes. The results are presented in Figures 12 through 15. The PID controller, shown with double-dashed green lines, exhibited instability, producing large oscillations and errors during high-activity periods, as depicted in Figure 12. Its fixed gains struggled with the rapid transitions of the multistep profile. The FPID controller, indicated by dashed green lines, improved tracking slightly, as shown in Figure 12, but persistent errors remained due to its limited ability to handle sudden changes. The FSMC controller, represented by double-dashed purple lines, outperformed PID and FPID, but disturbances caused oscillations and high errors, particularly

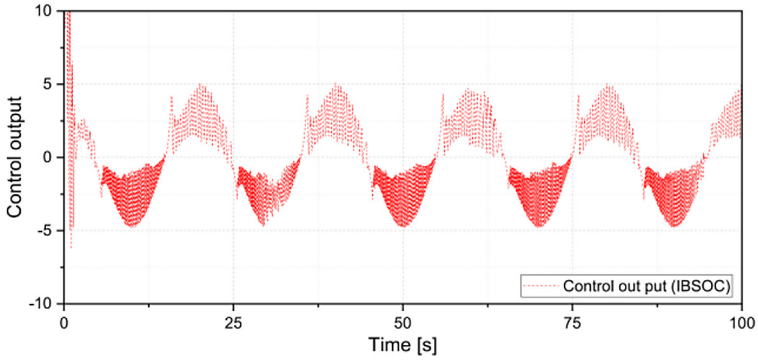

Figure 6. Control signal for a sinusoidal reference using the IBSOC controller, source: based on MATLAB/Simulink and AMESim co-simulation

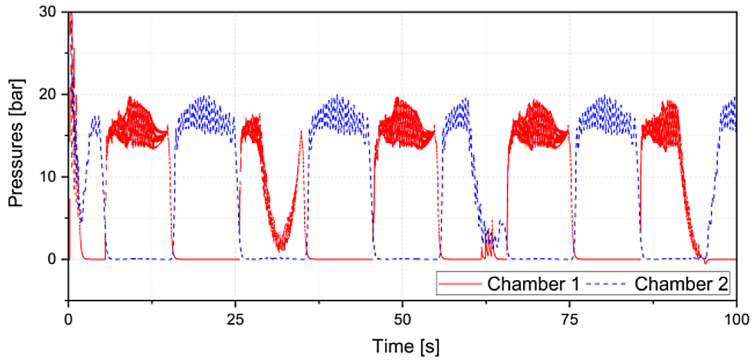

Figure 7. Pressure of EHRA's chambers (IBSOC controller) corresponding to a sinusoidal reference, source: based on MATLAB/Simulink and AMESim co-simulation

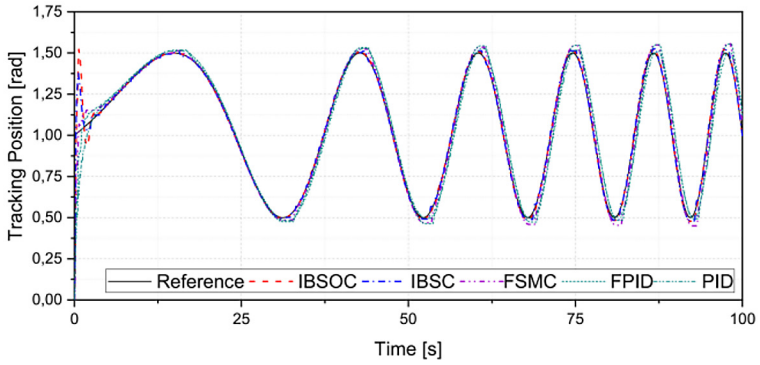

Figure 8. Comparison of tracking performance for a chirp reference using different controllers, source: based on MATLAB/Simulink and AMESim co-simulation

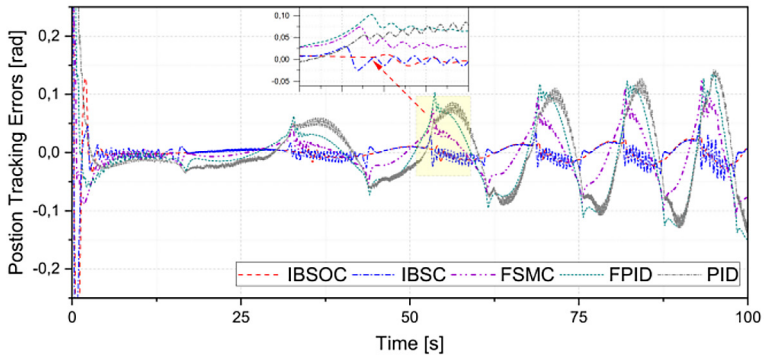

Figure 9. Comparison of tracking errors for a chirp reference using different controllers, source: based on MATLAB/Simulink and AMESim co-simulation

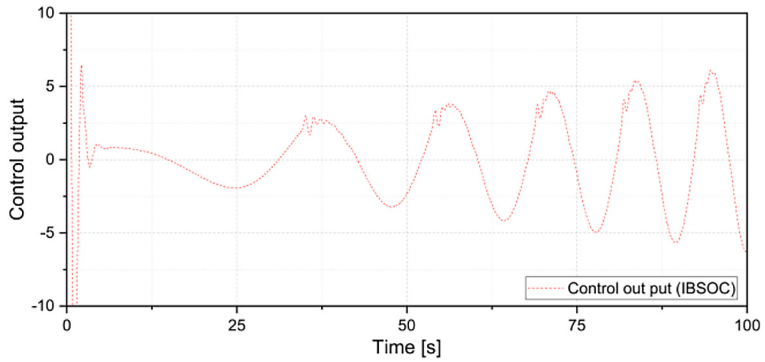

Figure 10. Control signal for a chirp reference using the IBSOC controller, source: based on MATLAB/Simulink and AMESim co-simulation

during step transitions, as illustrated in Figure 12. The IBSC controller, marked by dash-dotted blue lines, reduced steady-state errors through iterative learning, as seen in Figure 12, but oscillations in initial cycles and at step changes led to errors. Conversely, the IBSOC controller, depicted by dashed red lines, delivered fast, accurate, and stable responses, as shown in Figure 12. Its tracking errors, presented in Figure 13, were minimal. The motor control signals are displayed in Figure 14, and the actuator chamber pressures are shown in Figure 15. This case demonstrates the IBSOC's reliability in industrial scenarios requiring precise control over abrupt movements.

Finally, the sawtooth trajectory, characterized by sharp, linear changes, was evaluated to test the controllers' ability to handle demanding profiles. The results are shown in Figures 16

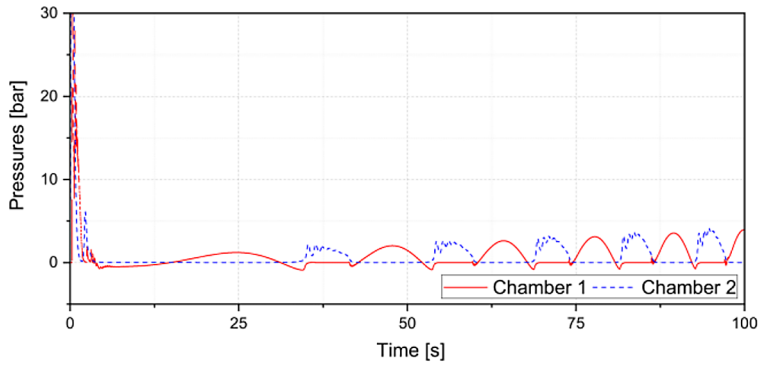

Figure 11. Pressure of EHRA's chambers (IBSOC controller) corresponding to a chirp reference, source: based on MATLAB/Simulink and AMESim co-simulation

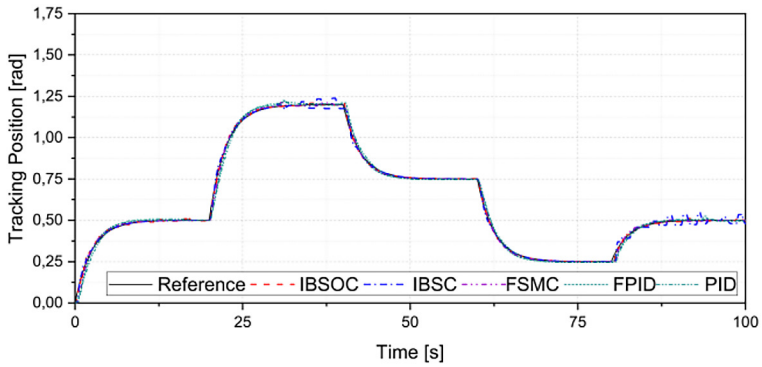

Figure 12. Comparison of tracking performance for a multi-step reference using different controllers, source: based on MATLAB/Simulink and AMESim co-simulation

through 19. The PID controller, illustrated by double dot-dashed green lines, exhibited notable instability with large oscillations and tracking errors during peak phases, as depicted in Figure 16. Due to fixed gains, the PID controller was unable to accommodate the trajectory's sudden shifts. The FPID controller, indicated by dashed green lines, demonstrated modest improvements in position tracking; however, the fuzzy logic component struggled with the trajectory's complexity, leading to substantial errors. The FSMC controller, represented by double dot-dashed purple lines, offered better performance overall, but still experienced oscillations and large errors, particularly at sharp transitions, as shown in Figure 16. The IBSC controller, marked by dash-dotted blue lines, reduced steady-state errors through iterative learning, as illustrated in Figure 16; nonetheless, oscillations remained during initial cycles and directional changes. In contrast, the IBSOC controller, depicted by dashed red lines, achieved rapid, accurate, and stable tracking, as shown in Figure 16. Its corresponding tracking errors, presented in Figure 17, were the lowest among all methods. Figures 18 and 19 illustrate the motor control signals and actuator chamber pressures, respectively. The integration of the IBSC framework with a self-tuning observer enabled the IBSOC controller to anticipate system dynamics and adjust control parameters proactively, thereby minimizing oscillations and errors under severe disturbances. These results highlight the reliability and effectiveness of the IBSOC approach in managing high-gradient motion trajectories in electro-hydraulic systems.

AB/Simulink and AMESim co-simulation

Controller performance was further analyzed in Table 1 using root mean square error (RMSE) and average relative error (ARE), defined in Equations (44–45). The IBSOC controller exhibited superior performance, with faster responses and lower errors, particularly under disturbances. By optimizing parameters in real time, the IBSOC

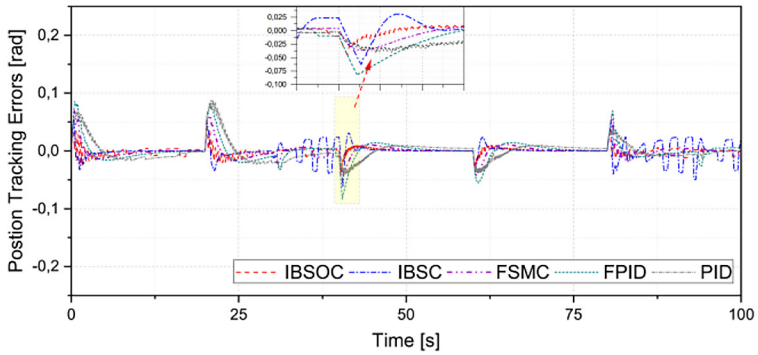

Figure 13. Comparison of tracking errors for a multi-step reference using different controllers, source: based on MATLAB/Simulink and AMESim co-simulation

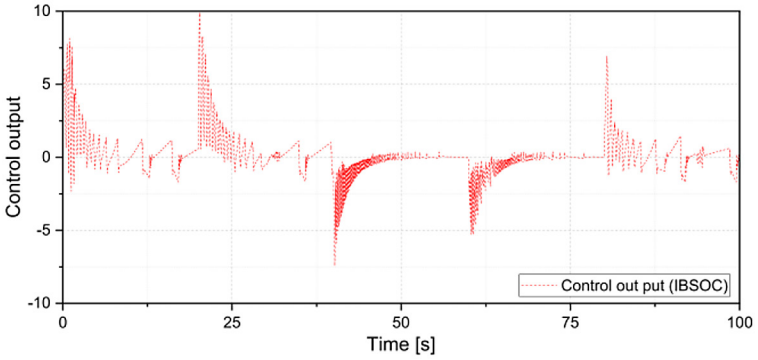

Figure 14. Control signal for a multi-step reference using the IBSOC controller, source: based on MATLAB/Simulink and AMESim co-simulation

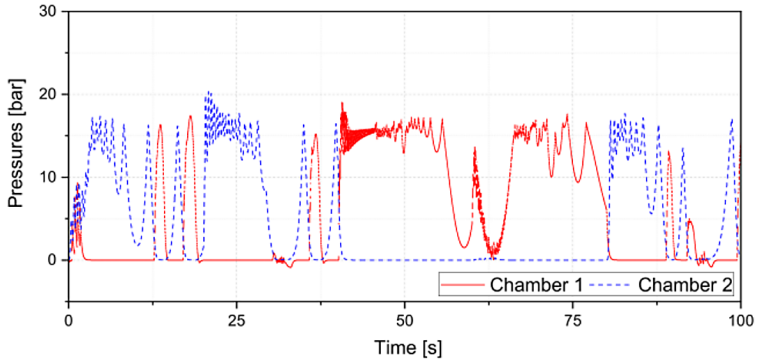

Figure 15. Pressure of EHRA's chambers (IBSOC controller) corresponding to a multi-step reference, source: based on MATLAB/Simulink and AMESim co-simulation

controller ensures precise tracking, minimizing oscillations and errors throughout operation.

$$\mathrm{RMSE} = \sqrt{\frac{1}{n}\sum_{k=1}^{n}\left(y_{in}(k) - y_{out}(k)\right)^2} \quad (44)$$

$$\mathrm{ARE} = \frac{1}{n}\sum_{k=1}^{n}\left(\frac{\left|y_{in}(k) - y_{out}(k)\right|}{y_{in}(k)} \times 100\right), [\%] \quad (45)$$

Across the sinusoidal, chirp, multistep, and sawtooth trajectories, the IBSOC controller consistently demonstrated superior performance compared to the PID, FPID, FSMC, and IBSC controllers in terms of speed, accuracy, and stability, with minimal tracking errors observed. The combination of real-time parameter adaptation and the predictive capability of the integrated observer enabled the IBSOC controller to maintain robustness under various disturbance conditions.

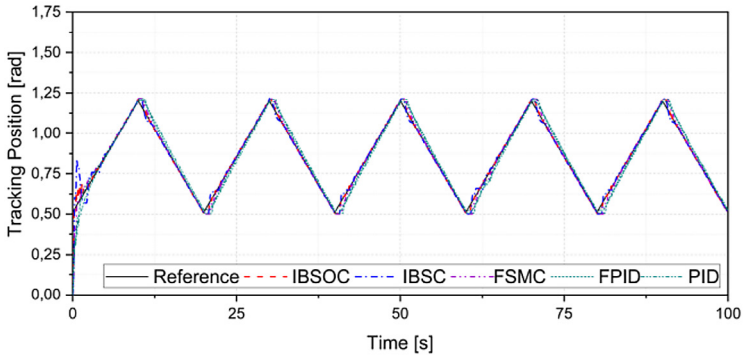

Figure 16. Comparison of tracking performance for a sawtooth reference using different controllers, source: based on MATLAB/Simulink and AMESim co-simulation

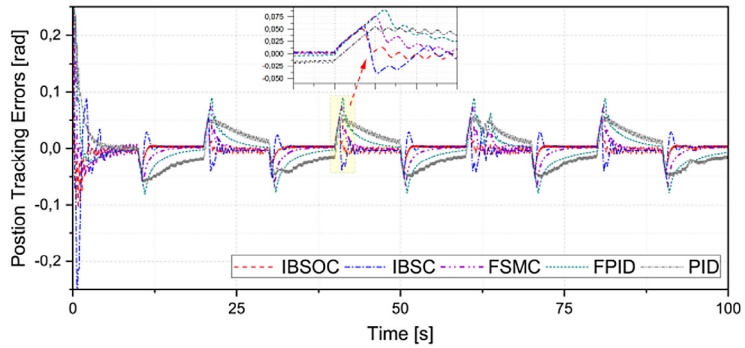

Figure 17. Comparison of tracking errors for a sawtooth reference using different controllers, source: based on MATLAB/Simulink and AMESim co-simulation

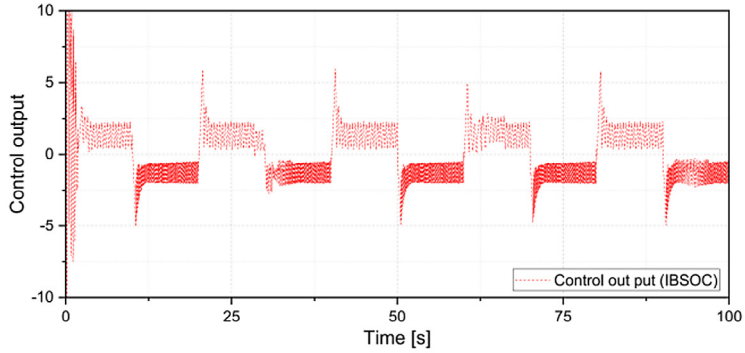

Figure 18. Control signal for a sawtooth reference using the IBSOC controller, source: based on MATLAB/Simulink and AMESim co-simulation

These results underscore the effectiveness of the proposed control scheme for complex electro-hydraulic applications requiring high precision.

Compared with conventional control approaches, the proposed hybrid control strategy also shows significant improvement in handling system nonlinearities and uncertainties. While traditional PID-based controllers often suffer from steady-state errors, and sliding mode controllers introduce undesirable chattering effects, the IBSOC offers smoother and more stable behavior. Although fuzzy-PID and adaptive backstepping methods enhance adaptability, they tend to underperform in state estimation and convergence rate under varying conditions. In contrast, our integration of ILC and nonlinear observation into a Lyapunov-stable backstepping framework offers a more balanced solution in terms of accuracy, robustness, and implementation feasibility.

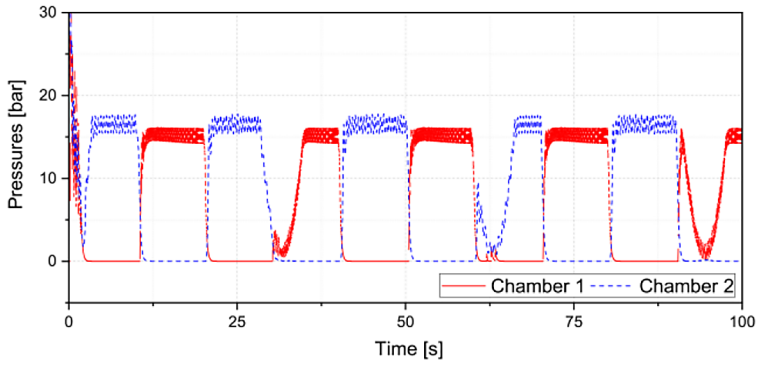

Figure 19. Pressure of EHRA's chambers (IBSOC controller) corresponding to a sawtooth reference, source: based on MATL

Table 1. Control performance evaluation

Validation		Evaluation criteria	
Case	Controller	RMSE [rad]	ARE [%]
Sinusoidal	PID	0.075583	0.055120
	FPID	0.068236	0.050544
	FSMC	0.051047	0.026163
	IBSC	0.064477	0.019360
	IBSOC	0.040785	0.013424
Chirp	PID	0.078579	0.053397
	FPID	0.074754	0.051745
	FSMC	0.057453	0.033420
	IBSC	0.046450	0.014621
	IBSOC	0.015423	0.010208
Multi-Step	PID	0.018332	0.030061
	FPID	0.018107	0.027376
	FSMC	0.012309	0.019179
	IBSC	0.013310	0.018031
	IBSOC	0.007169	0.011949
Sawtooth	PID	0.038569	0.037351
	FPID	0.038150	0.028977
	FSMC	0.030087	0.015601
	IBSC	0.030955	0.016088
	IBSOC	0.020085	0.009719

Note: Authors' calculations based on data provided by MATLAB/Simulink and AMESim co-simulation.

CONCLUSION

This study presents a novel position control method for pump-driven electro-hydraulic rotary actuator systems that addresses the challenges of nonlinearity, parameter uncertainty, and unmeasured states inherent in such systems. By integrating a modified backstepping algorithm, an iterative learning control scheme, and a state observer, the proposed hybrid control strategy achieves accurate position tracking while ensuring robustness and stability under a wide range of operating conditions. The method is validated through co-simulations in AMESim and MATLAB/Simulink, showing tracking errors below 0.5% and estimation errors within 1%. These results not only confirm the method's effectiveness but also provide practical insights into combining iterative learning and state estimation in nonlinear hydraulic systems. The approach offers high potential for precision motion control in industrial applications such as robotics, aerospace, and

heavy machinery. Although this study is based on simulation validation, future research will aim to implement the proposed control strategy in real time and evaluate its effectiveness through experimental testing on a physical testbench under realistic operating conditions.

Acknowledgement

We acknowledge Nguyen Tat Thanh University, Ho Chi Minh City, Vietnam and Ho Chi Minh City University of Industry and Trade, Ho Chi Minh City, Vietnam for supporting this study.

REFERENCES

1. Zhu J, Shen C, He Q, Li S, Dai P, Li X. Boom Potential Energy Regeneration Method for Hybrid Hydraulic Excavators. IEEE Access. 2024;12:51450–62. https://doi.org/10.1109/access.2024.3386741
2. Yao B., Zhang J., Koehler D. and Litherland J.. High performance swing velocity tracking control of hydraulic excavators. Proceedings of the 1998 American Control Conference. ACC (IEEE Cat. No.98CH36207), Philadelphia, PA, USA, 1998;818–822:2. https://doi.org/10.1109/ACC.1998.70352
3. Tri, N.M., Nam, D.N., Park, H.G., Ahn, K.K. Trajectory control of an electro hydraulic actuator using an iterative backstepping control scheme. Mechatronics, 2015;29:96–102. https://doi.org/10.1016/j.mechatronics.2014.10.002
4. Kumar P, Park S, Zhang Y, Jo SH, Kim HS, Kim T. A review of hydraulic cylinder faults, diagnostics, and prognostics. International Journal of Precision Engineering and Manufacturing-Green Technology. 2024;11:1637–61. https://doi.org/10.1007/s40684-024-00639-3
5. Liem DT, Huy NM, Nam LV, Nu HTM. An adaptive predictor-based control approach for tracking control of a hydraulic actuator system. Advances in Science and Technology – Research Journal. 2024;18(7):419–36. https://doi.org/10.12913/22998624/193862
6. Liem DT. Trajectory control of a hydraulic system using intelligent control approach based on adaptive prediction model. IFAC Journal of Systems and Control. 2023;26:100228. https://doi.org/10.1016/j.ifacsc.2023.100228
7. Mustafa D, Mehmet İS. Automation of friction torque identification for vane-type semi-rotary pneumatic actuators. Journal of the Brazilian Society of Mechanical Sciences and Engineering. 2023;45(6):340. https://doi.org/10.1007/s40430-023-04252-4
8. Yang M, Zhang X, Shi Y, Wang X. Mechanical design and position-tracking control of a novel robotic joint with a circular rotary electro-hydraulic actuator. Proceedings of the Institution of Mechanical Engineers, Part C: Journal of Mechanical Engineering Science. 2023;237(16):3680–91. https://doi.org/10.1177/09544062221148309
9. Liu R, Jin Z, Li X, Yuan L. Dynamic response characteristics of the hydraulic rotary system of an azimuth thruster for a dynamic positioning vessel. Journal of Marine Science and Engineering. 2023;11(2):399–9. https://doi.org/10.3390/jmse11020399
10. Yang M, Zhang X, Xia Y, Liu Q, Zhu Q. Adaptive Neural network-based Sliding Mode Control for a Hydraulic Rotary Drive Joint. Computers & Electrical Engineering. 2022;102:108189–9. https://doi.org/10.1016/j.compeleceng.2022.108189
11. Abdullah AM, Al-Samarraie SA, Ali HH, Al-Qassar AA. Design and Implementation of a Backstepping Time Varying Sliding Mode Control for the Angular Velocity Control of a Hydraulic Rotary Actuator. Journal of Robotics and Control. 2025;6(1):177–90. https://doi.org/10.18196/jrc.v6i1.24472
12. Liem DT, Truong DQ, Park HG, Ahn KK. A Feedforward Neural Network Fuzzy Grey predictor-based Controller for Force Control of an electro-hydraulic Actuator. International Journal of Precision Engineering and Manufacturing. 2016;17(3):309–21. https://doi.org/10.1007/s12541-016-0039-3
13. Qu S, Fassbender D, Vacca A, Busquets E. A high-efficient Solution for electro-hydraulic Actuators with Energy Regeneration Capability. Energy. 2021;216:119291. https://doi.org/10.1016/j.energy.2020.119291
14. Bobo Helian, Chen Z, Yao B. Constrained Motion Control of an Electro- Hydraulic Actuator under Multiple Time-Varying Constraints. IEEE Transactions on Industrial Informatics. 2023;19(12):11878–88. https://doi.org/10.1109/tii.2023.3249760
15. Ho TH, Le TD. Development and Evaluation of Energy-Saving Electro-Hydraulic Actuator. Actuators. 2021;10(11):302. https://doi.org/10.3390/act10110302
16. Liem DT, Truong DQ, Ahn KK. A Torque estimator using online tuning grey fuzzy PID for applications to torque-sensorless Control of DC Motors. Mechatronics. 2015;26:45–63. https://doi.org/10.1016/j.mechatronics.2015.01.004
17. Nguyen MT, Dang TD, Ahn KK. Application of electro-hydraulic actuator system to control continuously variable transmission in wind energy converter. Energies. 2019;12(13):2499. https://doi.org/10.3390/en12132499
18. Çetin Ş, Akkaya AV. Simulation and Hybrid fuzzy-PID Control for Positioning Of a hydraulic System. Nonlinear Dynamics. 2010;61(3):465–76. https://doi.org/10.1007/s11071-010-9662-1

19. Alleyne A, Liu R. A simplified approach to force control for electro-hydraulic systems. Control Engineering Practice. 2000;8(12):1347–56. https://doi.org/10.1016/S0967-0661(00)00081-2
20. Kalyoncu M, Haydim M. Mathematical Modelling and Fuzzy Logic Based Position Control of an Electro-hydraulic Servosystem with Internal Leakage. Mechatronics. 2009;19(6):847–58. https://doi.org/10.1016/j.mechatronics.2009.04.010
21. Filo G. A review of fuzzy logic method development in hydraulic and pneumatic systems. Energies. 2023;16(22):7584. https://doi.org/10.3390/en16227584
22. Dao TL, Ahn KK. Grey Prediction Based Adaptive Sliding Mode Control for electro-hydraulic Actuator System. In: 2015 15th International Conference on Control, Automation and Systems (ICCAS) IEEE; 201;857–61. https://doi.org/10.1109/iccas.2015.7364741
23. Guo X, Wang H, Liu H. Adaptive sliding mode control with disturbance estimation for hydraulic actuator systems and application to rock drilling jumbo. Applied Mathematical Modelling. 2024;136:115637–7. https://doi.org/10.1016/j.apm.2024.115637
24. Soon CC, Ghazali R, Ghani MF, Shern CM, Sam YM, Has Z. chattering analysis of an optimized sliding mode controller for an electro-hydraulic actuator system. Journal of Robotics and Control. 2022;3(2):160–5. https://doi.org/10.18196/jrc.v3i2.13671
25. Wang W, Zhou J, Wen C, Long J. Adaptive backstepping control of uncertain nonlinear systems with input and state quantization. IEEE Transactions on Automatic Control. 2021;67(12):6754–61. https://doi.org/10.1109/TAC.2021.3131958
26. Li Y, Tong S. Adaptive backstepping control for uncertain nonlinear strict-feedback systems with full state triggering. Automatica. 2024;163:111574–4. https://doi.org/10.1016/j.automatica.2024.111574
27. Cho B, Kim SW, Shin S, Oh JH, Park HS, Park HW. Energy-efficient hydraulic pump control for legged robots using model predictive control. IEEE/ASME Transactions on Mechatronics. 2022;28(1):3–14. https://doi.org/10.1109/tmech.2022.3190506
28. Shi Q, He L. A model predictive control approach for electro-hydraulic braking by wire. IEEE Transactions on Industrial Informatics. 2022;19(2):1380–8. https://doi.org/10.1109/TII.2022.3159537
29. Bahloul W, Zdiri MA, Marouani I, Alqunun K, Alshammari BM, Alturki M, et al. A backstepping control strategy for power system stability enhancement. Sustainability. 2023 Jun 2;15(11):9022–2. https://doi.org/10.3390/su15119022
30. Aguilar-Ibanez C, Acosta JÁ, Suarez-Castanon MS, Saldivar B, Moreno-Valenzuela EJ, Gandarilla-Esparza I, et al. Lyapunov-based estimation and control of velocity and load in rotating machines via luenberger globally-convergent observer. European Journal of Control. 2024;79:101092–2. https://doi.org/10.1016/j.ejcon.2024.101092
31. Zhou X, Wang H, Tian Y. Neural network state observer-based robust adaptive iterative learning output feedback control for the rigid-flexible coupled robotic systems with unknown delays and backlash-like hysteresis. Nonlinear Dynamics. 2022;110(2):1515–42. https://doi.org/10.1007/s11071-022-07713-y
32. Derrouaoui SH, Bouzid Y, Guiatni M. Adaptive integral backstepping control of a reconfigurable quadrotor with variable parameters' estimation. Proceedings of the Institution of Mechanical Engineers Part I Journal of Systems and Control Engineering. 2022;236(7):1294–309. https://doi.org/10.1177/09596518221087803
33. Ager P, Jimoh IA, Bevan G, Küçükdemiral I. Adaptive robust backstepping control based on radial basis neural network for linear motor drives. International Journal of Control. 2025;1–14. https://doi.org/10.1080/00207179.2025.2495124